

## Tomographic Imaging during Semi-Batch Reactive Precipitation of Barium Sulphate in a Stirred Vessel

T. L. Rodgers<sup>a\*</sup>, D. R. Stephenson<sup>a,b</sup>, M. Cooke<sup>a</sup>, T. A. York<sup>c</sup>, and R. Mann<sup>a</sup>

<sup>a</sup> School of Chemical Engineering and Analytical Science, University of Manchester, M60 1QD, UK; e-mail: T.Rodgers@postgrad.manchester.ac.uk

<sup>b</sup> current address: BP Chemicals, Salt End, Hull, HU12 8DS.

<sup>c</sup> School of Electrical and Electronic Engineering, University of Manchester, M60 1QD, UK

**Abstract.** The work reported in this paper has illustrated, for the first time, the capability of three-dimensional EIT to monitor reactive systems under realistic process conditions and scale. The semi-batch precipitation of barium sulphate from barium chloride and sodium sulphate has been investigated in a 200 litre stirred tank reactor. Experiments have been performed using both Rushton and pitched blade turbines under a range of agitation rates with a surface feed of barium chloride. The repeatability of EIT in monitoring the reaction progress has been illustrated. The visualisation of plume structure and evolution during the semi-batch reaction has been examined in 3D. The quantification of the effect of changes in reactor level on reconstructed images has also been examined suggesting this is a limitation to the commonly used finite element approach, as only a 2 % change can cause significant effects.

**Key words:** Tomography; Mixing; Precipitation; Multi-phase reactor; EIT

### 1. INTRODUCTION

Stirred tank reactors are often viewed as the workhorse of specialty, pharmaceutical and agrichemical processes [1]. There exist some unique challenges of production within stirred tank reactors in the pharmaceutical and agrichemical sectors, namely that there is a large degree of regulatory control over all production processes. In particular, features of this regulatory control are that operations are restricted to a narrow range of conditions, process changes directed towards process improvement are restricted [1]. Finally that most sensitive to these restrictions are probably those key mixing dependent processes such as crystallization and precipitation.

Despite their widespread use, stirred tank reactors often suffer from little (or no) instrumentation and a weak understanding of the often complex fundamental processes that take place within them. These processes can include reaction, mixing, extraction, distillation, and crystallization or precipitation. A significant challenge in the design and operation of stirred tank reactors is that processes such as fluid mixing, reaction and heat transfer all occur in the same vessel, often simultaneously, and the operating conditions optimal for one of these processes may not be optimal for the others.

One frequently encountered challenge in the design of stirred tank reactors occurs when the kinetics of the reaction are fast compared to the rate of mixing within the reactor. This scenario is indicated by a large Damkohler number (the ratio of characteristic mixing time to reaction time). The contacting of reagents impacts on all scales of mixing, mass transfer, reaction and ultimately can impact on selectivity, yield and solid product characteristics such as particle size distribution and morphology for heterogeneous systems. Precipitation

reactions are well known to be dependent on many variables, including reaction stoichiometry, feed mode, feed rate, feed location, temperature, seeding, impurities, and mixing intensity [2].

In addition to the modelling of mixing sensitive reaction systems, there have been many studies reporting the measurement of flow and mixing using various methods. Examples of these methods include Hot Wire Anemometry (HWA), Laser Doppler Anemometry (LDA), Laser Doppler Velocimetry (LDA), Phase Doppler Anemometry (PDA), Particle Image Velocimetry (PIV), Planar Laser-Induced Fluorescence (PLIF), and Positron Emission Particle Tracking (PEPT).

This paper presents, for the first time, the application of true three-dimensional Electrical Impedance Tomography (EIT) to monitor the semi-batch precipitation of barium sulphate from barium chloride and sodium sulphate within a stirred tank reactor. The precipitation of barium sulphate has been widely studied in order to investigate the impact of mixing on the particle size distribution and particle morphology and to validate numerical models of mixing sensitive reactive precipitation [3]. EIT is one of the few measurement methods that is able to investigate the reaction environment within stirred tank reactors fully, where both significant spatial and temporal variation in property distributions are coupled with optical inaccessibility. In particular, EIT provides the potential to visualize the non-uniformity in electrical conductivity caused by spatial variation in mixing intensity, the meso-scale inhomogeneity of the addition plume and agitator-generated macro-scale flow loops.

## 2. EXPERIMENTAL EQUIPMENT AND PROCEDURES

### 2.1 Experimental Equipment

The precipitation experiments were carried out in a 0.610 m diameter ( $T$ ), flat-based, baffled stirred tank reactor. The vessel has four equally spaced baffles and can be fitted with a Rushton turbine (RT) or a pitched blade turbine (PBT). The vessel was filled to a liquid level of  $0.91T$ , providing a semi-tech scale-up version of the vessel used by Stanley [4] (from 6.6 to 160 litres). The vessel is fitted with 8 rings of 16 equally spaced EIT electrodes in a baffle cage configuration. Figure 1 illustrates a schematic diagram of the vessel arrangements.

The ITS P2000 was chosen for the experiments presented in this paper as it is the best performing EIT instrument, available to us, for experiments requiring high temporal resolution and is capable of successfully monitoring homogeneity [5]. Table 1 summarises the data acquisition settings employed during the experiments. The optimal injection current was found to be 75 mA resulting in a signal-to-noise ratio (SNR) of approximately 55 dB at a

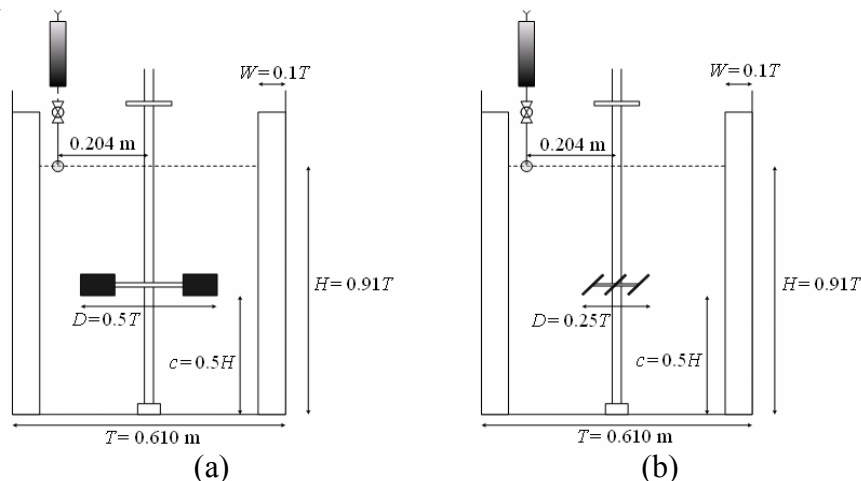


Figure 1. Schematic representation of the stirred tank reactor geometry for the precipitation experiments using (a) Rushton turbine and (b) pitched blade turbine.

Table 1. ITS P2000 data acquisition settings.

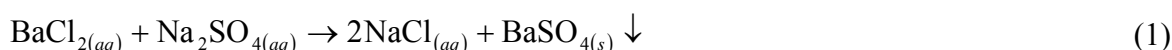
Setting	Value
Excitation frequency, kHz	9.6
Sampling time interval, ms	40
Samples per frame	1
Frames per download	Equal to the maximum number of frames
Delay cycles	3
Injection current, mA	75
Sampling strategy	Normal adjacent

reactor charge conductivity of  $0.075 \text{ S m}^{-1}$ . Only the upper six planes of electrodes were used in the experiments, due to voltage data asymmetry issues arising from the proximity of the tank base to the bottom two levels [6]. The collected voltage data was reconstructed using a GSVD algorithm [7] based on a finite element model comprising 8886 elements. The regularisation parameter in the algorithm was chosen to be the maximum value obtained by an analysis of the Discrete Picard Condition [8] for all frames captured during the experiment.

For the three-dimensional images presented, all which use the same colour scale, the minimum value is the starting conductivity of the sodium sulphate charge ( $0.075 \text{ S m}^{-1}$ ) and the maximum value is the maximum of the global mean conductivity trajectory ( $0.084 \text{ S m}^{-1}$ ). Four isosurfaces have been selected, at one-quarter intervals across the conductivity range starting at the first quartile and ending at the maximum of the colour scale, i.e. 25%, 50%, 75% and 100% of the range. The opacity of the isosurfaces has been graded such that the lower conductivity isosurfaces are less opaque than those of higher conductivity, enabling a see-through quality to the visualization.

## 2.2 Experimental Procedures

The precipitation of barium sulphate from barium chloride and sodium sulphate proceeds by the reaction described in Equation (1).



All experiments were carried out using a 1:1 stoichiometric ratio of reagents. A 2 l feed of barium chloride ( $\text{BaCl}_2 \cdot 2\text{H}_2\text{O}$ , ACS grade, Fisher Scientific) at a concentration of  $0.2 \text{ mol l}^{-1}$  was made up in deionised water. The sodium sulphate ( $\text{Na}_2\text{SO}_4 \cdot 10\text{H}_2\text{O}$ , ACS grade, Fischer Scientific) charge at a concentration of  $2.25 \times 10^{-3} \text{ mol l}^{-1}$  was made up in mains water to a volume of 160 l. The barium chloride was fed into the reactor in 65 seconds using a peristaltic pump, representing a feed rate of  $2 \text{ l min}^{-1}$ . The feed was introduced into the reactor on the charge fluid surface, midway between two baffles at a distance of 67% of the vessel radius from the agitator shaft. Care was taken to ensure that the reagent solutions were at a constant temperature during the experiments.

Agitation rates for the PBT were calculated on a scale up basis of geometric similarity and equal power input per unit volume from the power inputs used earlier at laboratory scale by Stanley [4]. The agitation rates for the RT were also calculated at the same power per unit volume, in order to perform a comparison of the two agitators. The agitation rates used were 25, 50, 100, 150, 225, 305, and 380 rpm for the  $45^\circ$  PBT and 8, 16, 25, 38, and 51 rpm for the RT. Each of these speeds were repeated at least twice.

### 3. RESULTS

#### 3.1 Repeatability

Figure 2 shows typical repeatability for the EIT derived parameters for the semi-batch process. The global conductivity is calculated as the mean of the conductivity of the entire set of 8886 elements comprising the finite element model, and the coefficient of variation (CoV) is calculated as the percent standard deviation over the mean.

Figure 2(b) shows that prior to the barium chloride feed, the CoV in the reactor is at a low value as only the initial homogeneous sodium sulphate charge is present. Under ideal conditions the CoV initially would be zero, however, due to the SNR of the EIT instrument (55 dB) the initial CoV is ~0.4%. The barium chloride feed is started at approximately 25 seconds and Figure 2(a) shows that the global conductivity within the reactor starts to increase due to the higher conductivity of the more concentrated feed. The conductivity continues to increase reasonably linearly until the feed addition stops at approximately 90 seconds, indicating a feed time of 65 seconds. From Figure 2(b) the CoV begins to increase as a feed plume of high conductivity barium chloride develops, creating a spatial variation in conductivity within the reactor. The CoV reaches a peak value of 8.5% at approximately 40 seconds, 15 seconds after the feed period started. For the remainder of the feed period, the CoV remains high (~7% to ~8.5%).

It can be seen from Figure 2 that after the feed addition ceases at 90 seconds, the global conductivity starts to decay almost exponentially, as does the CoV, towards the final conductivity of the reaction products. This process represents the final plume of barium chloride being dispersed in the reactor and consumed by the reaction described by Equation (1). The difference between the initial CoV (0.4%) when homogeneous and the end CoV when the reactor is assumed homogeneous (2%) can be explained by the non-linear instrument response of the ITS P2000 [5] and the change in vessel level due to the semi-batch feed.

The very similar global conductivity trajectories between the two runs indicate that the experiment has a very good degree of repeatability.

#### 3.2 Effect of Agitation Speed

Figure 3 shows the global conductivity trajectories for the various agitation rates used with the Rushton turbine and the pitched blade turbine. It is clear from Figure 3 that there exists significant variation in the trajectories through the range of rates investigated, while the semi-batch feed times are fairly constant across the range of experiments. The end point of the feed period can be readily obtained from Figure 3 by examining the exact point at which the global conductivity begins to decay to the final value.

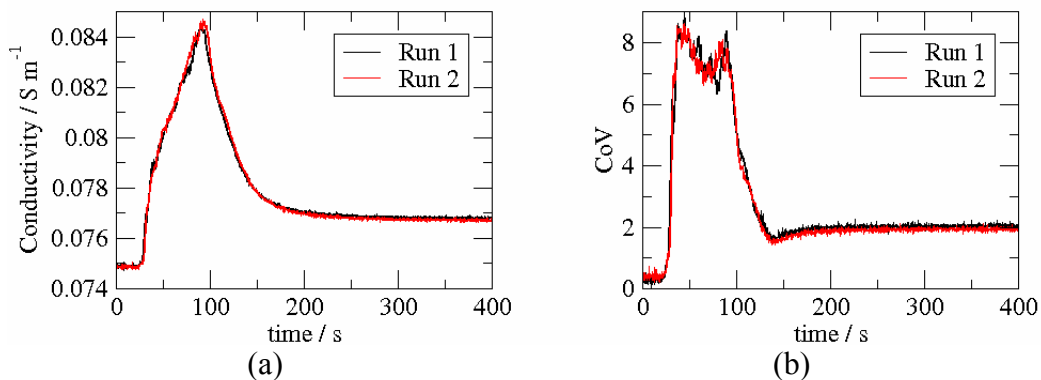


Figure 2. (a) Global conductivity and (b) CoV trajectories for two repeat runs using the Rushton turbine at 8 rpm.

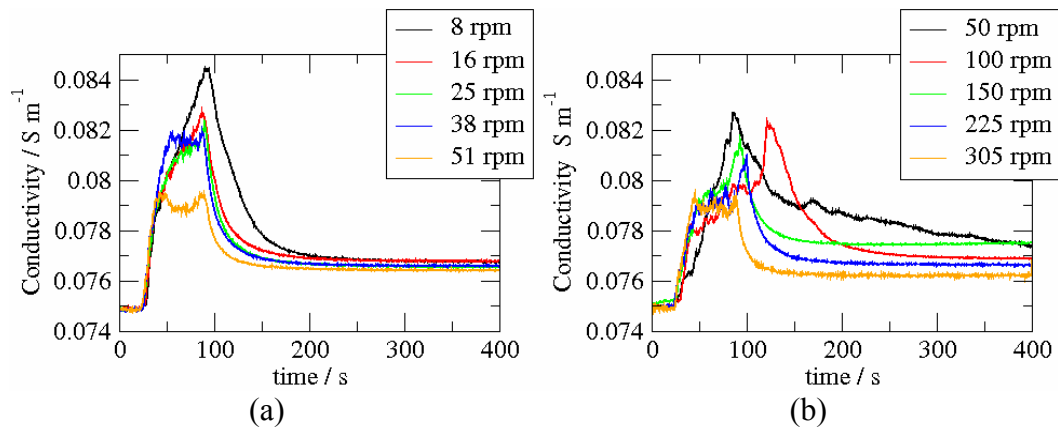


Figure 3. Global conductivity trajectory averaged over repeat experiments for the (a) Rushton turbine at 8, 16, 25, 38, and 51 rpm and (b) Pitched blade turbine at 50, 100, 150, 225, and 305 rpm.

The peak value of the global conductivity appears to decrease with increasing agitation rate for both agitators; this is due to the barium chloride feed plume being less well dispersed at lower agitation rates, thus less is consumed by the precipitation reaction, resulting in a higher global conductivity.

Figure 3 also suggests that an interesting transition occurs over the range of agitation rates investigated. At 8 rpm for the RT and 50 rpm for the PBT, little of the barium chloride is consumed by reaction during the feed period due to relatively poor mixing, shown by the almost linear increase in global mean conductivity. As the agitation rate increases (16→25 rpm RT, 100→150 rpm PBT), Figure 3 shows that the global conductivity trajectory becomes less linear, with a reducing gradient towards the end of the feed period. This suggests that some of the barium chloride feed is being consumed by reaction, therefore the global conductivity does not increase to the extent demonstrated by the 8 rpm (RT) and 50 rpm (PBT) case. At the higher speeds (38→51 rpm RT, 225→305 rpm PBT) the global conductivity trajectory reaches a plateau approximately 30 seconds into the feed period. This plateau indicates that the addition of high conductivity barium chloride by the semi-batch feed is approximately balanced by the consumption of barium chloride by the precipitation reaction.

### 3.3 Analysis of Flow Patterns

Figure 4 (a) and (i) show the initial homogeneous mixture in the vessel at  $0.075 \text{ S m}^{-1}$  for the Rushton turbine and the pitched blade turbine respectively. Figure 4 (b) and (j) show the start of the addition period and both have a slightly higher conductivity at the top of the vessel where the feed has been injected. Figure 4 (c) and (k) are at about 6 seconds into the feed time; the global conductivity is starting to increase significantly and the feed plume has now been set up within the reactor. Figure 4 (c) and (d) also show the development of the barium chloride up and down the vessel wall following the typical flow loop of a Rushton turbine. It is apparent that the barium chloride is experiencing a tangential swirl following the direction of the agitator in a clockwise direction. Figure 4 (k) and (l) show the flow development for the pitched blade turbine, initially the up-pumping flow holds the plume near the top and then the axial flow loop starts to extend the barium chloride distribution to the base of the vessel.

Figure 4 (e) and (m) show the end of the addition period. Figure 4 (e) and (f) show that the barium chloride has been fully distributed around the base of the vessel due to the tangential swirl, and the top of the vessel is starting to become more homogeneous. Figure 4 (m) and (n) show that the large area of high conductivity on the left is dissipating through the tank, with the bottom right area being the last to be dispersed. Figure 4 (g) and (o) show the vessel nearing its homogeneous value for both types of agitator, producing the end point ((h) and

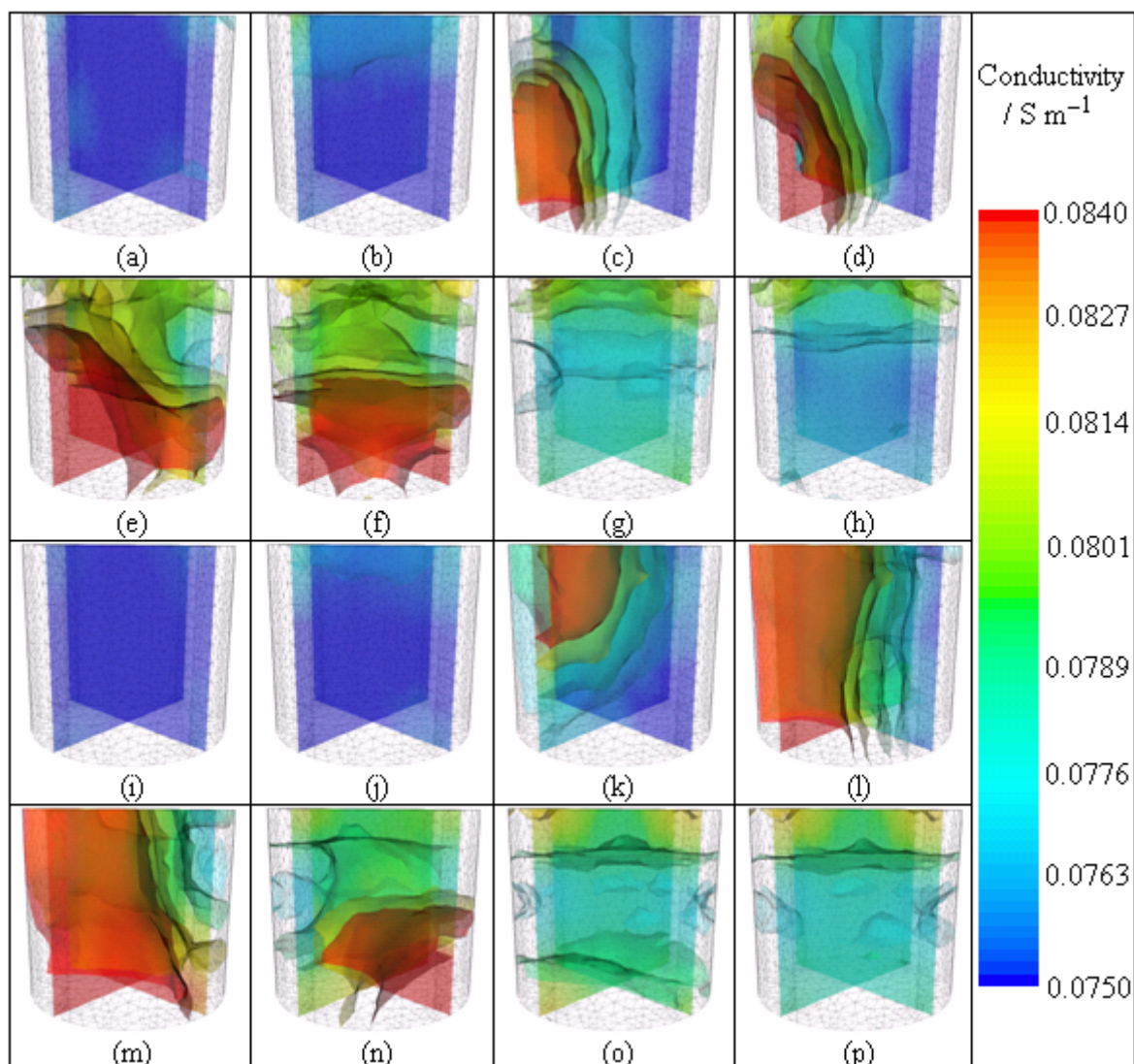


Figure 4. Visualisation of flow patterns for the Rushton turbine at (a) 10, (b) 25, (c) 31, (d) 44, (e) 90, (f) 100, (g) 140, and (h) 240 s at 8 rpm and for the pitched blade turbine at (i) 10, (j) 25, (k) 31, (l) 44, (m) 90, (n) 115, (o) 240, and (p) 350 s at 50 rpm.

(p)), of average conductivity of  $0.077 \text{ S m}^{-1}$ . Both (h) and (p) show a slight inhomogeneity at the top of the vessel. This inhomogeneity is due to level effects (see section 3.4) as this area never becomes homogeneous like the rest of the tank which it would if it was just due to weak circulation; also this effect is not seen if a small volume tracer is added.

### 3.4 Effects of Level Change

The majority of industrially relevant semi-batch reactions undergo a change in level during the progression of the process. This feature of the process causes a significant challenge to the current state-of-the-art in EIT. A series of simulated experiments have been undertaken in order to assess the impact of level changes on the reconstructed image and errors in the global mean conductivity within a vessel. The aim of the experiment was to verify that the regions of higher conductivity reconstructed (towards the top of the vessel) in the precipitation experiments presented were an image artefact. It is believed that this artefact is caused by the level change due to the semi-batch feed of barium chloride. An illustrative example of the level change artefact is seen in Figure 4(p). The addition of a 2 l feed of barium chloride into the 160 l charge of sodium sulphate increases the height of the reactor contents by 1.24%.

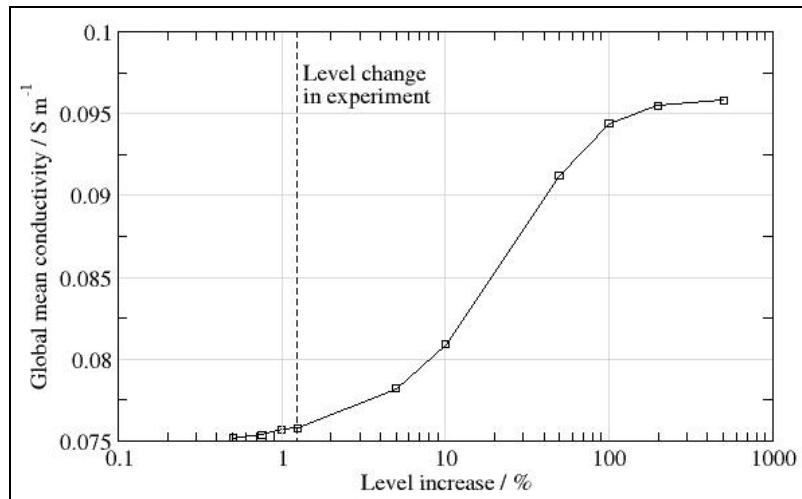


Figure 5. The effect of an increase in fluid level, at a constant conductivity of  $0.075 \text{ S m}^{-1}$ , on the global mean conductivity derived from the reconstructed image.

The effect of a change in level was investigated using a single plane of electrodes, simulating the top plane of electrodes used in the precipitation experiments. A series of geometric models were constructed, representing increases in level from 0.25 to 500% from the starting level. The simulated experiments were carried out at the same experimental conditions as the precipitation experiments presented, i.e. adjacent drive strategy, background conductivity of  $0.075 \text{ S m}^{-1}$  and 75 mA injection current. Although the average conductivity varied during the real precipitation experiment, the conductivity was held constant at  $0.075 \text{ S m}^{-1}$  in the simulated experiments so that the increase in level could be investigated independently. Figure 5 shows the effect of increasing the level of fluid in the vessel on the EIT-derived global mean conductivity.

Figure 5 demonstrates that small increases in the fluid within the vessel affect the EIT predicted mean conductivity only slightly. The reason that the conductivity is increased from  $0.075 \text{ S m}^{-1}$  is that an increase in the fluid level results in more volume for the electric field to penetrate. This results in the field strength reducing around the electrodes as the field is less confined, therefore voltage measurements are lower. Considering Ohm's law, if the voltage reduces at a constant current, the apparent resistance decreases and this in turn results in an increase in observed conductivity.

At the increase in fluid level experienced in the precipitation experiments reported in this paper, 1.24%, the EIT-derived mean conductivity is  $0.0758 \text{ S m}^{-1}$  representing a 1.1% error from the true conductivity of  $0.075 \text{ S m}^{-1}$ . Figure 5 shows that as the percentage change in level increases further, the error in the EIT derived mean conductivity increases. Eventually, the increase in fluid level starts to have less of an impact on the EIT mean conductivity as the electric field, at the constant injection current of 75 mA, penetrates the upper regions less. This is demonstrated in Figure 5 by the tailing off of the curve at level increases in excess of 200%.

The impact of fluid level changes in stirred vessels is clearly an area in which further work is required. It may be possible to include the fluid height as a priori information in the reconstruction algorithm and one possibility is to include the level variable in the state evolution approach as developed by Vauhkonen *et al.* [9].

#### 4. CONCLUSIONS

- Three-dimensional EIT has been used to monitor reactive systems under realistic process conditions and scale using both Rushton and pitched blade turbines under a range of agitation rates, for the first time.

- Metrics such as global conductivity and coefficient of variation have been calculated and used to track the reaction trajectory, alongside the three-dimensional conductivity distribution within the reactor.
- The repeatability of true three-dimensional EIT in monitoring the reaction progress has been illustrated.
- Three-dimensional EIT has enabled the plume evolution and structure to be visualised during the progression of the reaction. Results have demonstrated the variation in plume structure and evolution caused by the different flow patterns generated by the radial and axial impellers.
- The effect of a change in reactor level caused by the semi-batch feed has been reported for the first time and results indicate that current reconstruction techniques in EIT are extremely sensitive to a change in level.

## ACKNOWLEDGEMENTS

David Stephenson would like to thank EPSRC and Syngenta for financial support during his Engineering Doctorate. The authors would like to thank the SCEAS workshop staff who helped with equipment modifications and construction.

## NOMENCLATURE

<i>C</i>	Conductivity / S m <sup>-1</sup>	CoV	Coefficient of variation
<i>c</i>	Agitator clearance / m	PBT	Pitch blade turbine
<i>D</i>	Agitator diameter / m	RT	Ruston turbine
<i>H</i>	Liquid height / m	SNR	Signal to noise ratio
<i>T</i>	Vessel diameter / m		
<i>W</i>	Baffle width / m		

## REFERENCES

1. Paul, E.L., Atiemo-Obeng, V.A., & Kresta, S.M. (Eds.), 2004. *Handbook of Industrial Mixing: Science and Practice*, John Wiley & Sons Inc., New Jersey, USA.
2. Kagoshima, M. And Mann, R. , 2005. "Interactions of Precipitation and Fluid Mixing with Model Validation by Electrical Tomography", *Chem. Eng. Res. Des.*, **83**, 806-810.
3. Wong, D.C.Y., Jaworski, Z., & Nienow, A.W., 2001. "Effect of ion excess on particle size and morphology during barium sulphate precipitation: An experimental study", *Chem. Eng. Sci.*, **56**, 727-734.
4. Stanley, S., 2006. "Tomographic imaging during reactive precipitation in a stirred vessel: Mixing with chemical reaction", *Chemical Engineering Science*, **61**, 7850-7863.
5. Stephenson, D.R., York, T.A., & Mann, R., 2007. "Performance and requirements of process EIT instruments" *Proc. 5th World Congress on Industrial Process Tomography*, Bergen, Norway, 895-901.
6. Stephenson, D.R., 2008. "Choices and Implications in Three-Dimensional Electrical Impedance Tomography", EngD Thesis submitted to the University of Manchester.
7. Hansen, P. C., 1998. "Rank-Deficient and Discrete Ill-Posed Problems: Numerical Aspects of Linear Inversion", SIAM, Philadelphia, USA.
8. Hansen, P. C., 1990. "The Discrete Picard Condition for Discrete Ill-Posed Problems", *BIT Numerical Mathematics*, **30**, 658-672.
9. Vauhkonen, M., Vadasz, D., Karjalainen, P.A., Somersalo, E., & Kaipio, J.P., 1998. "Tikhonov regularization and prior information in electrical impedance tomography", *IEEE Tran. Medical Imaging*, **19**, 285-293.